Ultrasound backscatter tensor imaging (BTI): analysis of the spatial coherence of ultrasonic speckle in anisotropic soft tissues

Clement Papadacci, Mickael Tanter, Mathieu Pernot, Mathias Fink

UltrasoundBackscatter Tensor Imaging (BTI):

Analysis of the spatial coherence of ultrasonic speckle in anisotropic soft tissues

Clement Papadacci[1], Mickael Tanter[1], Mathieu Pernot[1*], Mathias Fink[1*]

* Co-last authors

[1]Institut Langevin, ESPCI ParisTech, Paris, 75005 France;

[1]CNRS, UMR 7587, Paris, 75005 France;

[1]INSERM, U979, Paris, 75005 France;

[1]Université Paris Diderot-Paris 7, Paris, 75013 France;

Corresponding address: papadacci.clement@gmail.com

Institut Langevin, ESPCI

1 rue Jussieu, 75005 Paris, France

Tel: +33 1 80 96 33 43

Manuscriptreceived …

C. Papadacci, M. Tanter, M. Pernot and M. Fink are with Institut Langevin, Ecole Superieure de Physique et Chimie Industrielles (ESPCI), CNRS UMR 7587, INSERM, U979, 75005, Paris, France and withUniversité Paris Diderot-Paris 7, 75013, Paris, France

Abstract

The assessment of fiber architecture is of major interest in the progression of myocardial disease. Recent techniques such as Magnetic Resonance (MR) Diffusion Tensor Imaging or Ultrasound Elastic Tensor Imaging (ETI) can derive the fiber directions by measuring the anisotropy of water diffusion or tissue elasticity, but these techniques present severe limitations in clinical setting. In this study, wepropose a new technique, the Backscatter Tensor Imaging (BTI) whichenables determining the fibers directions in skeletal muscles and myocardial tissues, by measuring the spatial coherence of ultrasonic speckle. We compare the results to ultrasound ETI.Acquisitions were performed using a linear transducer array connected to an ultrasonic scanner mounted on a motorized rotation device with angles from 0° to 355° by 5° increments to image *ex vivo* bovine skeletal muscle and porcine left ventricular myocardial samples. At each angle, multiple plane waves were transmitted and the backscattered echoes recorded. The coherence factor was measured as the ratio of coherent intensity over incoherent intensity of backscattered echoes. In skeletal muscle, maximal/minimal coherence factor was found for the probe parallel/perpendicular to the fibers. In myocardium, the coherence was assessed across the entire myocardial thickness, and the position of maxima and minima varied transmurally due to the complex fibers distribution. In ETI, the shear wave speed variation with the probe angle was found to follow the coherence variation. Spatial coherence can thus reveal the anisotropy of the ultrasonic speckle in skeletal muscle and myocardium. BTI could be used on any type of ultrasonic scanner with rotative phased-array probes or 2-D matrix probes for non-invasive evaluation of myocardial fibers.

Index Terms :

anisotropy, fiber, myocardium, spatial coherence, plane wave imaging, coherent compounding

I. Introduction

The structure of the heart wall iscomplex.The orientation of the myofibersvaries smoothly and continuously through the wall thickness[1]. This specific fiber architecture is relatedto mechanical[2–4]and electrical[5–8] properties of the myocardium. Therefore, imaging the fiber architecture *in vivo*is of major interest in the understanding of cardiac function and in the progression of myocardial diseases.

Opticalimaging modalities such as optical coherent tomography [9] or two-photon microtomy[10]can image the microscopic structure but with low penetration capabilities and are thus limited to the mapping of superficial structures. Other imaging tools such as Magnetic Resonance Diffusion Tensor Imaging (MR-DTI)[11],[12]have also been used to map the myocardial fiber structure, but mostly in *ex vivo* tissues. DTI can also measure the fiber orientation*in vivo*[13–15]but this remains challenging to perform in human patients because of long acquisition times.

In contrast, ultrasonic imaging modalitiesenable real-time visualization of the heart. Echocardiography is routinely employed in clinical practice to examine the heart motionandto provide estimations of the global cardiac function such as cardiac output, derived from the measure of diastolic and systolic ventricular volume [16]. Ultrasound can also be used to characterize the myocardial structure, through the analysis of backscattered ultrasound. The dependence of backscattered intensity and ultrasound attenuation with fiber orientation was investigated extensivelyover the past decades[17–20]. Nevertheless,backscattered intensity depends on many parameters including heterogeneity of the material, presence of bright specular echoes,angle view and period in the cardiac cycle.Therefore, clinical implementation of these techniques remains challenging.

Ultrasound and MR elastography techniques have also been proposed for mapping the anisotropy of the elastic properties in fibrous soft tissues[21],[22]. Because elastic properties of biological tissues are linked to the microstructure organization, elastic anisotropy can provide information on the fiber organization. Shear Wave Imaging (SWI), an ultrasound based technique that can map quantitatively the elastic properties of soft tissues in real-time[23], was used to determine the fiber directions in skeletal muscle[22]and myocardium[24–26].The propagation of shear waves was measured along several directions to determine the anisotropy of the shear modulus and the fibers direction. SWI has been employed *in vivo*on the beating

heart[27–30]to derive myocardial stiffness and contractility estimation [27],[28] and was used to determine the fiber orientation *in vitro* in porcine myocardial samples [24],[25] and *in vivo* in open-chest animals [24],[26]. This technique, named Elastic Tensor Imaging (ETI) was shown to provide comparable information on the fiber direction as DTI in a small region of an *ex vivo* heart tissue [26].Despite the potential interest of anisotropic elastic estimates for cardiac pathologies screening or diagnosis, an important limitation of this technique for future fiber tracking clinical applications is the need of generating a shear waveat every locations of interest, which require long acquisitions.

Another way to characterize the tissue microstructure with ultrasound, is to analyzethe spatial coherence of the backscattered echoes. Spatial coherence characterizes the level of similarity of backscattered signals received by two different distant elements of an ultrasonic probe. The spatial coherence of backscattered signals provide information on the distribution of scatterers within a focal region. In a random distribution of scatterers, Van Cittert-Zernike showed that spatial coherence of light was dependent only on the size of the focal zone. This result was extended to the field of pulse echo ultrasound by Fink and Mallart [31]. In the field of diagnostic ultrasound, spatial coherence has been extensively investigated in many applications including aberration corrections[32–35]and reduction of the clutter signal in B-mode images [36],[37].Additionally, Derode et al.[38] proposed to use the spatial coherence information to characterize the scatterers distribution in composite materials. They estimated the spatial coherence of the backscattered signals on a linear array along different directions and found a higher spatial coherence when the linear array was oriented along the fibers than across them. Therefore, we assumed that spatial coherencecould also reveal the fibers orientation in soft biological tissues, and we introduce here a new technique called Backscatter Tensor Imaging (BTI) to characterize the human tissue microstructure. This approach takes advantage of ultrafast ultrasound imaging [39]based on plane wave transmissions in order to strongly decrease the number of transmissions required to assess the backscatter tensor information. This is mandatoryto ensure a clinical applicability of the technique in a dynamic imaging mode.

In this study, weinvestigated the anisotropy of spatial coherence in fibrous tissues. First, a technique was developed to map rapidly the spatial coherence in 2D using alimited number of plane wave transmits. The anisotropy of the spatial coherence was then evaluated by rotating the ultrasonic probe. Experiments were performed in *ex vivo*bovine muscles and porcine myocardial samples. The results obtained with BTI

werecomparedtothe anisotropy of elastic modulus provided by Elastic Tensor Imaging. This technique has the potential of imaging in real-time the three-dimensional (3D) microstructure of fibrous tissues.

II. MATERIAL AND METHODS

A. Spatial coherence in random media and in anisotropic materials

1) Spatial coherence in random media: The Van-Cittert Zernike theorem

In conventional ultrasound imaging, an ultrasound pulseis focused in the region of interest (Figure 1(a)). The ultrasound field backscattered by the random distribution of scatterersis received on all the array elements (Figure 1(b)) and appear mostly coherent at large distance from the focus. The spatial coherencecharacterizes the similarity between the signalsreceived by two distant elements of the array.VanCittert-Zernike determined the degree of coherence by defining a coherence function as the averaged cross-correlation between two signals received at two points of space. As the distance between elements increases, the degree of coherence decreases. The so-called Van Cittert-Zernike theorem states that the coherence function is the spatial Fourier transform of the intensity distribution at the focus. Therefore a focus generated by a rectangular aperture provides a triangle coherence function[31], (Figure 1(c)).

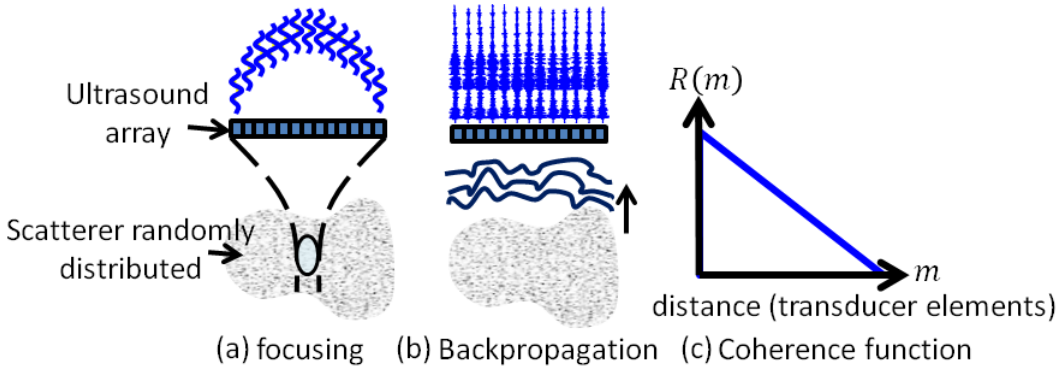

Fig.1. Principle ofspatial coherence assessment in a random media. An ultrasound pulse is focused in the biological tissue with an ultrasonic probe (a). The backscatter echoes are received on the array (b). The coherence function R(m) is computed using cross-correlations performed between pairs of transducer elements distant by m (c).

The coherence function$R$is assessed as a function of distance in number of elements m (or lag)by making auto-correlations between all pairs of receiver elements([38]):

$$R(m) = \frac{N}{N-m}\frac{\sum_{i=1}^{N-m} c(i,i+m)}{\sum_{i=1}^{N} c(i,i)}, \quad (1)$$

where N is the number of elements of the array and $c(i,j)$ is defined as:

$$c(i,j) = \sum_{T_1}^{T_2} (S_i(t) - \bar{S_i})(S_j(t) - \bar{S_j}) , \quad (2)$$

where$[T_1 T_2]$ is the temporal window centered on the focal time, $S_i$is the time-delayed signal received on transducer i and $\bar{S_k}$ is defined as follow:

$$\bar{S_k} = \frac{1}{T_2 - T_1} \sum_{T_1}^{T_2} S_k(t), \quad (3)$$

The degree of spatial coherence can also be evaluated by another parameter,the ratio of coherent intensity over incoherent intensity, the so called Mallart-Fink focusing factor orcoherence factor *C*[33],[34], defined as:

$$C = \frac{\sum_{T_1}^{T_2} \left| \sum_{i=1}^{N} S_i(t) \right|^2}{N \sum_{i=1}^{N} \sum_{T_1}^{T_2} |S_i(t)^2|} , \quad (4)$$

2) Coherence in anisotropic media

Derode et al.in [38] demonstrated that the coherence function*R* varied with the fiber direction in anisotropic composite solid materials (e.g. Figure 2(a)). An ultrasound linear transducer mounted on a rotation devicewas used to evaluate the coherence function along different directions.Across the fibers,the coherence function was found to be a triangle (e.g. Figure 2(b) blue curve) whereas the degree of coherence increased along the fibers (e.g. Figure 2(b) red curve). Indeed, across the fibers, the scatterers appears randomly distributed; but along the fibers, scatterers are distributed preferentially along them which backscatters the transmitted beam more coherently.

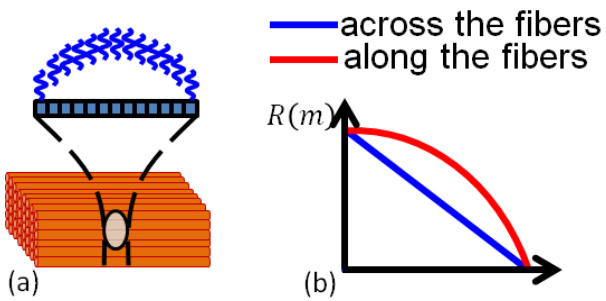

Fig.2. Principles of spatial coherence in anisotropic media. Along the fibers (red curve), backscattered signals are more coherent than across the fibers (blue curve) and coherence function tends to increase.

B. Experimental setup and data acquisition

1) Mapping the spatial coherence using plane wave coherent compounding

Spatial coherence evaluation as described above requires to focus an ultrasound pulse within a region of interest. However, soft tissues are highly inhomogeneous in terms of tissue composition which implies the presence of inhomogeneities in spatial coherence. In fact, spatial coherence can be affected by strong specular scatterers. Specular scatterers increase spatial coherence locally and can occur both along the fibers and across the fibers. In such tissues, the coherence function or coherence factor has to be averaged. In order to map the spatial coherence overa larger region, the ultrasonic beam must be focused successively at different locations.However, a large number of focused transmits may strongly affect the frame rate and therefore limit the clinical development of this technique.

In order to reduce the number of transmits for real-time implementation; we propose here to use plane wave coherent compounding. The principle relies on the transmission of several plane waves with the full aperture at different incident angles[40]. Then, by applying coherent summation of the backscattered waves,a focus issynthetized everywhere in the imaging plane (e.g. Figure 3).

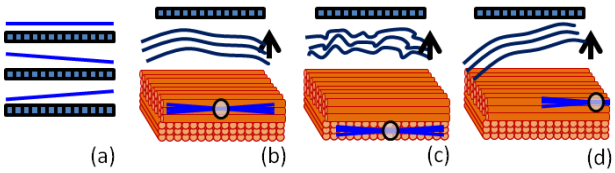

Fig.3. Three tilted plane waves are sent successively by an ultrasonic linear transducer. Each plane wave is backscattered by heterogeneities and the array receives the corresponding echoes. Synthetic focus is processed by making coherent summation of the plane waves at the focal point with the adequate delays (b). By changing the delay applied to each backscattered echoes from (a), the resulting waves can bevirtually focused at different depth (c) and lateral positions (d).

By synthesizinga focus at each point of the imaging plane, the spatial coherence of corresponding backscattered echoes can be evaluated everywhere.Therefore, it allows mapping the spatial coherence of the entire 2D imaging plane using a small number of transmits. A mean coherence degree can be computed over a region of interest (e.g. Figure 4).

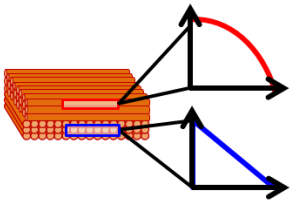

Fig.4. Plane wave coherent compounding allows spatial coherence estimationeverywhere in the imaging plane with a small number of transmits. It can provide 2D mapping of coherence function using a small number of transmits.

To compare the performances of plane wave coherent compounding in BTI with the number of plane waves, we added successive plane waves with a small angular pitch. With this configuration, the lateral resolution (linked to the angular extent) increased with the number of plane waves and at the same time the grating lobes are minimized.

Moreover, coherent plane wave compounding providesthe same synthetic focus everywhere in the image in transmit. It is equivalent to a constant F-number (F/ D) in transmit. Therefore, in order to compare easily the spatial coherence at different locations of the image, the F-number in receive should be kept constant by adapting the receive aperture (D). In this study the F-number was fixed to 1.5 with an associated lateral resolution of 385µm in receive.

2) Experimental Set up

a) Spatial coherence in an imaging phantom

Spatial coherence with plane wave coherent compounding was first evaluated in an imaging phantom (ATS, model 551) with hypoechogenic inclusions of varying sizes, a sound speed of 1450 m/s at 23° and an attenuation coefficient of 0.5 dB/cm/MHz.A linear transducer array (6MHz, 128elements, 0.2mm pitch, 100% bandwidth, Vermon, France) connected to a programmable ultrasonic scanner (Aixplorer, SuperSonic Imagine, France) was used. A number of 41 tilted plane waves (from -20° to 20° with a step angle of 1°) were transmitted in the phantom. The 41 RF backscattered signals received by each transducer elements weredigitized with a sampling frequency of 24MHz and stored in memory, no apodization was used. Coherent summation of the RF signals was performed for each temporal points.After backpropagation,

coherencefactors were calculated according to equation (4)at each sampling point. The averaging window $[\boldsymbol{T_1 T_2}]$was set tofour periods at 6MHz corresponding to a time of about 0.67µs.

The dependence of spatial coherence with the number of tilted plane waves was investigated by increasing the number of plane waves in the coherent summation: one plane wave at 0°, 5 plane waves (-2°,-1°,0°,1°,2°), 11 plane waves (from -5° to 5°), 21 plane waves (from -10° to 10°) and finally 41 plane waveswere investigated. Conventional normalized B-mode imagesand coherence B-mode images corresponding to thelocal coherence factors are presented for each case.

b) Spatial coherence in soft tissues

Acquisitions were performed on 3 *ex vivo* bovine skeletal muscles and 3 porcine left ventricle myocardial samples embedded in agar-gelatin (2%-2%) phantom. Acquisitions were performed using the same linear transducer array as previously connected to the same ultrasonic scanner. The probe was mounted on a motorized rotation device with angles varying from 0° to 355° by 5° increments. At each probe angle, 41 tilted plane waves from -20° to 20° (with a step angle of 1°)were transmitted and the backscattered echoes recorded. RF signals were stored on a computer and time delayed at each point of space. Coherent compounding was performed using the 41 plane waves. Compounded RF signals were then used to calculate coherence functions with respect to equation (1) and coherence factorsaccording to equation (4) at each point of space.Distance was normalized on the abscissa axisof coherence functions by the number of elements used in reception with respect to the F-number of 1.5.

3) Fiber angle estimation: Backscatter Tensor Imaging (BTI)

In soft tissues,the coherence factor was averaged around the central axis of the image, at each depth, over a small area (the lateral dimension was 4 mm and the axial dimension was 1 mm). Thisparameter represents the degree of spatial coherence over a region with a given lateral and axial extension and was defined as theSpatially Averaged Coherence Factor (SACF). SACF was estimated at each depth as a function of probe angle. The angle of the fiber was assigned to the probe angle for which the SACF was at its maximum.

4) Fractional anisotropy

For an anisotropic medium the fractional anisotropy (FA)was calculated at each depth as:

$$\mathbf{FA} = \frac{\sqrt{\mathbf{2}}\sqrt{(\mathbf{C}_{//} - \bar{\mathbf{C}})^{\mathbf{2}} + (\mathbf{C}_{\perp} - \bar{\mathbf{C}})^{\mathbf{2}}}}{\sqrt{\mathbf{C}_{//}{}^{\mathbf{2}} + \mathbf{C}_{\perp}{}^{\mathbf{2}}}}, \quad (5)$$

where $\mathbf{C}_{//}$ is the value ofSACFalong fibers, $\mathbf{C}_{\perp}$ is the value ofSACFacross fibers and $\bar{\mathbf{C}}$ isthe mean SACF over probe angles. FA allows the evaluation of the degree of anisotropy of the backscatter properties.FA quantifies the degree of anisotropy of a medium with respect to a technique.This parameter varies between 0 (isotropic medium) to 1.

C. Elastic Tensor Imaging (ETI)

1) Principle

Elastic tensor imaging was used here as a validated technique to determine the fiber direction in anisotropic tissue. The principle relies on the fact that shear waves propagate the fastest along the fibers and the slowest across the fibers.Lee et al [24] has also demonstrated that shear wave imaging has the sensitivity to detect the complex fiber orientation in myocardium as a function of depth. This technique has been called ETI (elastic tensor imaging). ETI has also been correlated with DTI (diffusor tensor imaging) in the myocardium [26]. We propose in this study to use ETI to validate results from BTI.

2) Acquisition

ETI acquisitions were performed during the BTI experiments using the same probe. At each probe angle, just after BTI acquisition, Shear Wave Imaging was performed.40 frames were acquired to image the propagation of a shear wave induced by the acoustic radiation force of a focused ultrasound burst (duration 300µs, focused at 20mm depth for the bovine muscles and 30 mmfor the myocardial samples with anF-number of 1.5) at 8,000 frames per second.

3) Fiber angle estimation

Tissue velocities were obtained using a per pixel frame to frame 1D cross-correlation on demodulated IQ images with an axial kernel size of 3 pixels (385 µm) to obtain images of tissue frame-to-frame axial displacements. At each depth, shear wave speedswere estimated by tracking the maxima of tissue velocities along time in a small region laterally around the focal spot (4mm). Shear wave speeds were evaluatedfor each probe angle.At each depth, the fiber orientation was derived by detecting the maximum shear wave

speed with respect to probe angles.For each sample, Spearman's rank correlation coefficient (ρ)on fiber orientation estimated by ETI and BTI was calculated to compare the two techniques.

III. RESULTS

A. Imaging phantom

Spatial coherence using plane wave coherent compounding was evaluated in the imaging phantom as a function of the number of plane wave transmits.In the top row ofFigure 5,normalized B-mode images are shown for increasing number of plane waves (e.g. (a),(c),(e),(g)). Improvement of both contrast and resolution is noticed by increasing the number of plane wave transmits as shown by [40].Signal to noise ratio (SNR) is estimated as described above (part. B.2.a) and averaged on the small and the large inclusions (e.g. Figure 6(b)). The blue curve on Figure 6(a), shows an improvement of about 10dB when 41 plane wavesare used (e.g. Figure 5(g)) compared to 1 (e.g. Figure 5(a)).

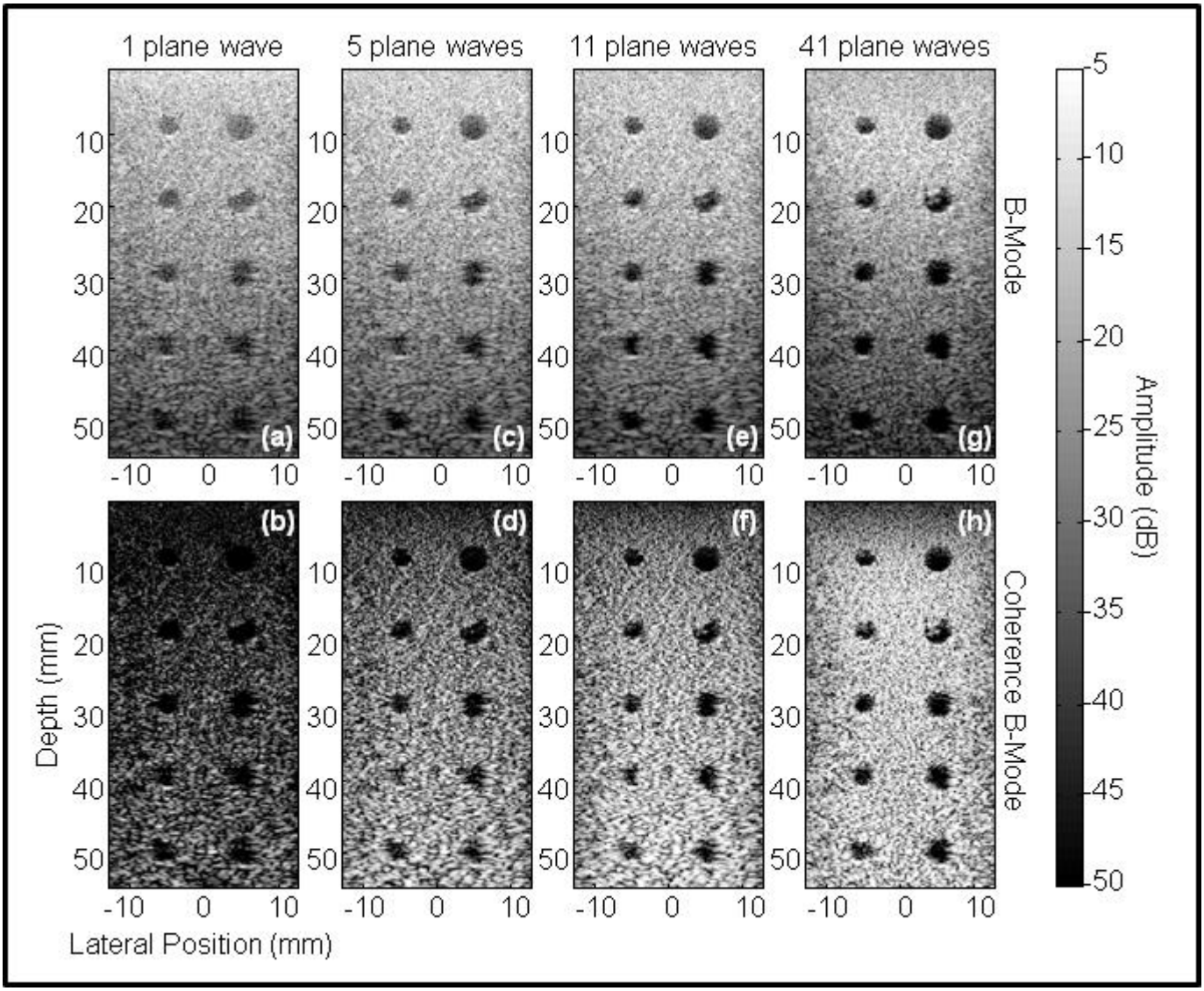

Fig.5. Comparison between B-mode images (a),(c),(e),(g) and Coherence B-mode images (b),(d),(f),(h), for one plane wave (a),(b) and increasing number of plane waves used in the coherent compounding process: 5 plane waves (c),(d), 11 plane waves (e),(f), 41 plane waves (g),(h).

Coherence B-mode images are displayed in the bottom row of Figure 5(e.g. (b),(d),(f),(h)). The degree of coherence becomeshigher with the number of plane waves meaning a higher spatial coherence obtained by animprovement of the synthetic focusing quality.

B. *Ex vivo* bovineskeletal muscles

1) BTI measurement

BTI was first validated on skeletal muscles. In skeletal muscle fibers are mostly oriented in the same direction and fiber orientation is visible on B-mode images which is useful to know the orientation of the probe(e.g. bright line onFigure 6(a)).The coherence function$\boldsymbol{R(m)}$was found to varywhen the probe was oriented across the fibers (blue curve) compared to the probe oriented along them (red curve). Figure 6(c) shows coherence functionsaveraged overdepth from 10 mm to 30 mm (e.g. green rectangle Figure 6(a)) and associated standard deviations.

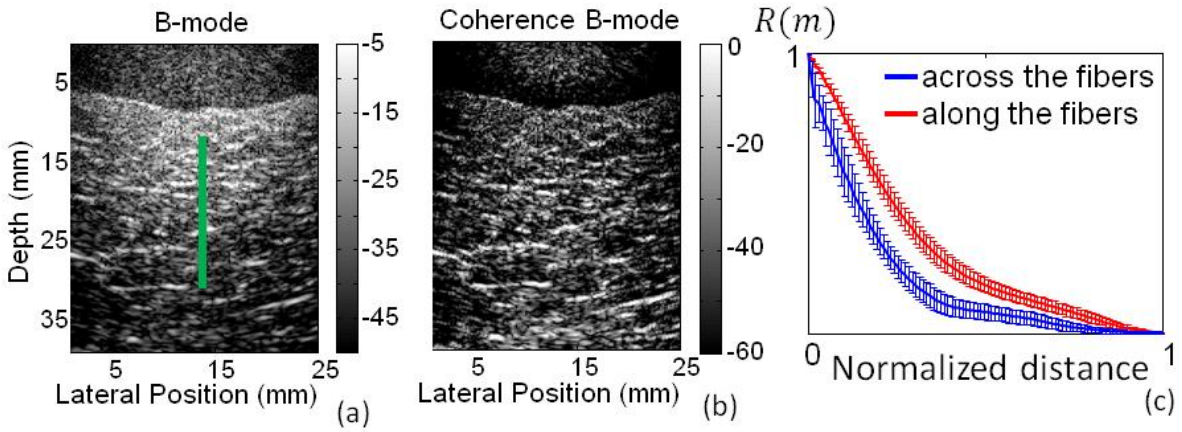

Fig.6. 41 plane waves B-mode image (a) and Coherence B-mode image (b) of a bovine skeletal muscle. Coherence functions are calculated across the fibers (c)-blue curve and along the fibers (c)-red curve. The distance (transducer elements) varies with depth z, and is equal to z/F-number. It was normalized with respect to a F-number of 1.5.

The SACF was then calculated as described in part II-B-3. It was calculated on the central axis for each probe angle. Figure 7(a) shows an example of SACF variation at a 20.5mm depth as a function of probe

angle. The maxima of the curve give the parallel direction to the fibers (blue arrow) whereas minima give the transverse direction to the fibers (green arrow).

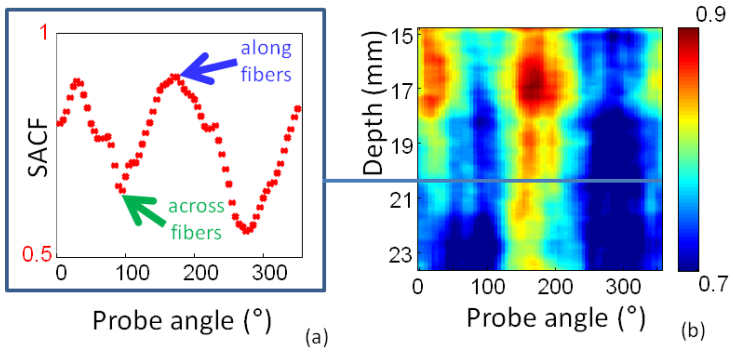

Fig.7. SACF variation with probe angle in skeletal bovine muscle,at a depth of 20.5 mm (a). The maximal SACF is obtained when the probe is parallel to the fibers (blue arrow). The minimal SACF is obtained when the probe is perpendicular to the fibers (green arrow). Fiber direction can be assessed at each depth (b).

The SACF variation was assessed as a function of probe angle at each depth and the fiber direction was assigned to the probe angle for with maximal SACF. As expected the fiber direction was found to be nearly the same as a function of depth.

The fractional anisotropy was calculated, as described previously, for all samples and averaged: FA = 0.46 (+/- 0.05).

2) Validation of BTI against ETI

The fiber direction wasalso measured using ETI. The procedure is described in part II-C. At each probe angle and each depth,the shear wave speed (SWS)was assessed in a small region laterally around the focal spot. It was found to varyin average from1.9 (+/-1) m/s across the fibers up to 4.1 (+/-1) m/s along the fibers with FA = 0.42 (+/- 0.07). Figure 8 shows an example at a 20.5mm depth. A good agreement was found between estimations of fiber directions made with BTI and with ETI. The agreement was quantified by a Spearman correlation between ETI and BTI on the estimations of fiber directions over depth. In average, over the three samples, the correlation coefficient was $\rho = 0.92 \pm 0.04$.

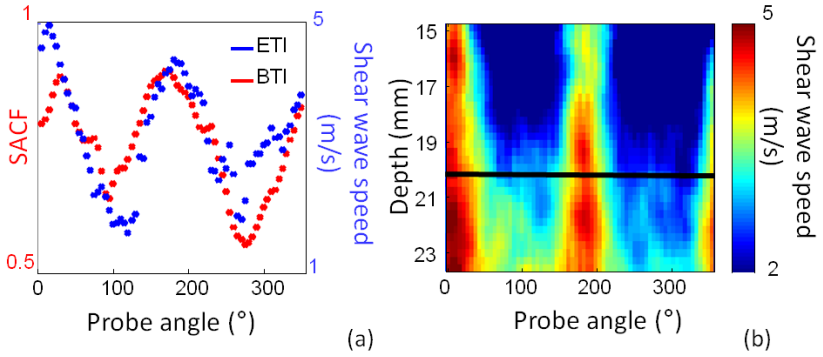

Fig.8.Validation of BTI against ETI at a depth of 20.5 mm (black line on (b)). The SACF is represented for BTI, the shear wave speed is represented for ETI (a). Fiber direction can be assessed at each depth with ETI (b).

C. In*ex vivo* myocardial samples

1) BTI measurement

The myocardium is a much more complex anisotropic soft tissue compared to skeletal muscle. The fibers are not visible on focused B-mode images (e.g. Figure 9(a)) and their orientations change transmurally[1].The coherence function was shown to vary with fiber angle through the myocardium. For each depth, the direction of fibers was assessed by tracking the maxima of the coherence factor. Then corresponding parallel and perpendicular coherence functions were averaged along depth. Figure 9(b) displays averagedcoherence function when the probe is set along the fibers (red curve) and across the fibers (blue curve).The coherence function is higher along the fibers (red curve) than across the fibers (blue curve).

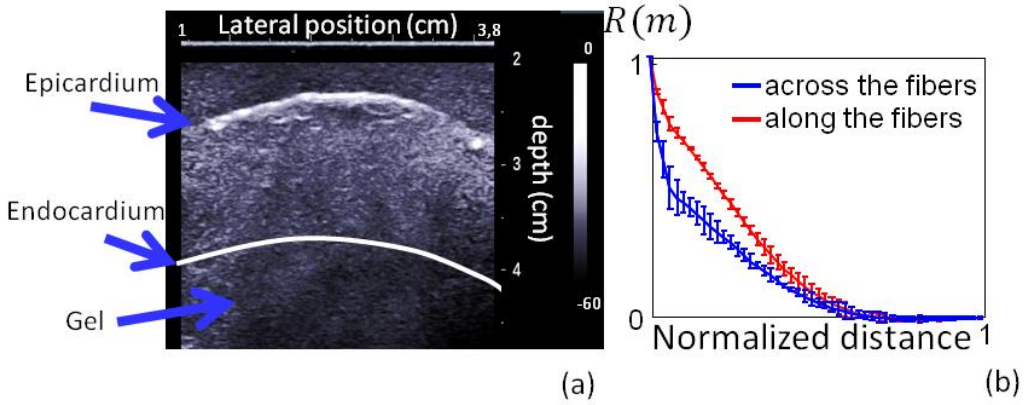

Fig.9. Focused B-mode image of a porcine myocardial sample embedded in a gel (a). Coherence functions $\boldsymbol{R}(\boldsymbol{m})$ *across the fibers (b)-blue curve and along the fibers (b)-red curve are averaged over depth of a myocardial sample.*

SACFwas also found to vary with probe angle (Figure 10(b)). The maxima and minima of SACFwere also shown to vary with depth. Figure 10(b) displays an example of SACF variation in one myocardial sample as a function of probe angle and at three different depths. The red curve represents the SACF at sub-epicardium (e.g. Figure 10(a) red rectangle), the green curve at midwall (e.g. Figure 10(a) green rectangle) and the blue curve at sub-endocardium (e.g. Figure 10(a) blue rectangle). The SACF variation can be imaged as a function of probe angle and depth through the myocardial wall (wall thickness) (e.g. Figure 10(c)). This maxima shift gives a different fiber orientation as a function of depthas expected.

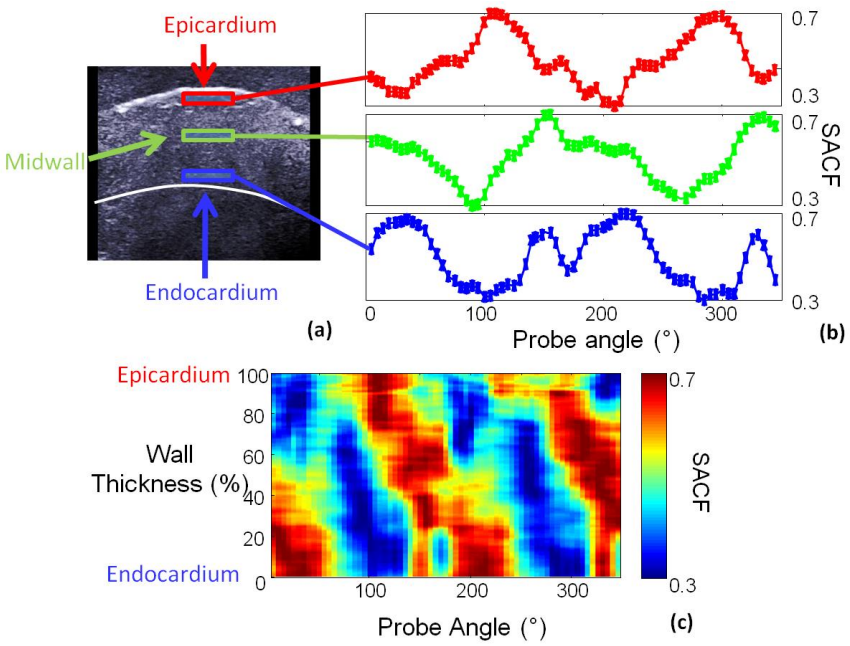

Fig.10. Three locations on the focused B-mode image of a myocardial sample (a) and the associated variation of SACF (b) are presented. SACF is imaged as a function of probe angle at each depth through the myocardial sample (Wall thickness in (%)) (c). Maxima at each depth give to the fiber angle variation as a function of wall thickness.

The probe angle that corresponds to the maximum SACFwas estimated at each depth. The fiber directions estimated with BTI, over the three samples, are represented in figure 11(a),(c),(e). Fibers were found to vary transmurally, from approximately -55° near the epicardium to +60° near the endocardium.

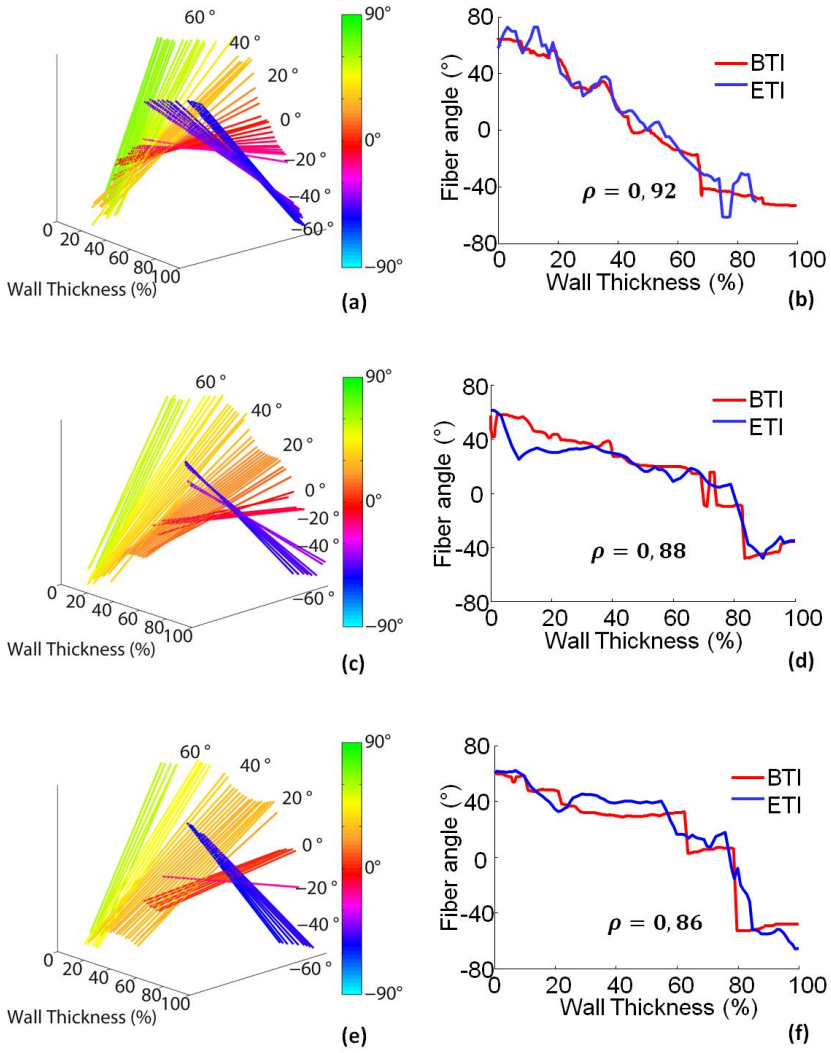

*Fig.11. The comparison of the fiber orientation estimated by BTI and ETI. The BTI fiber orientation plots are presented for the three myocardial samples (a),(c),(e). 0% and 100% wall thickness represent the endocardium and the epicardium, respectively. The angle value at midwall is set to 0°. The colorbar displays the fiber angles (from -90° to 90°). The fiber angle as a function of wall thickness estimated by BTI and ETI is compared in (b),(d),(e) for the three samples respectively and Spearman's rank correlation coefficient (**ρ**) is calculated to compare BTI and ETI fiber angle estimation.*

The fractional anisotropy was also calculated over the 3 samples and found to be: FA = 0.42 (+/- 0.05).

2) Validation of BTI against ETI

The fiber direction was also obtained by ETI. The shear wave speed was found to vary from 3.1m/s across the fibers to 5.9m/s along the fibers. The shear wave speed variation with the probe angle was found to follow mostly the spatial coherencevariation at each depth.

The estimation of fiber directionprovided by the two methods were also compared on the three myocardial samples (e.g. Figure 11(b),(d),(f)) and show a good agreement. Spearman correlation between ETI and BTI on the estimation of fiber directions over all porcine myocardial samples was calculated. We found in average: $\rho = 0.89 \pm 0.03$.

3) BTI measurement witha small number of transmitted plane waves.

With the same set of data, SACF was calculated for different number of plane waves used in the coherent compounding process. Figure 12 displays the results of SACF for 1,5,11,21 ((a),(b),(c),(d) respectively) compared to 41 plane waves (e) in a myocardial sample at each depth (22 mm to 36 mm).To compare the results, a normalization was applied to set the maximum of coherence to 1 and minimum to 0.5. Spearman correlation was performed to compare the fiber angles derived with ETI compared to BTI for the 5 different configurations. Spearman correlation's coefficient was plotted against the number of plane wave use in the coherent summation (e.g. Figure 12 (f)).

The results show a degradation of fiber angle estimation as the number of plane waves decrease but the anisotropy is observed in all acquisitions ($\rho \geq 0.6$).

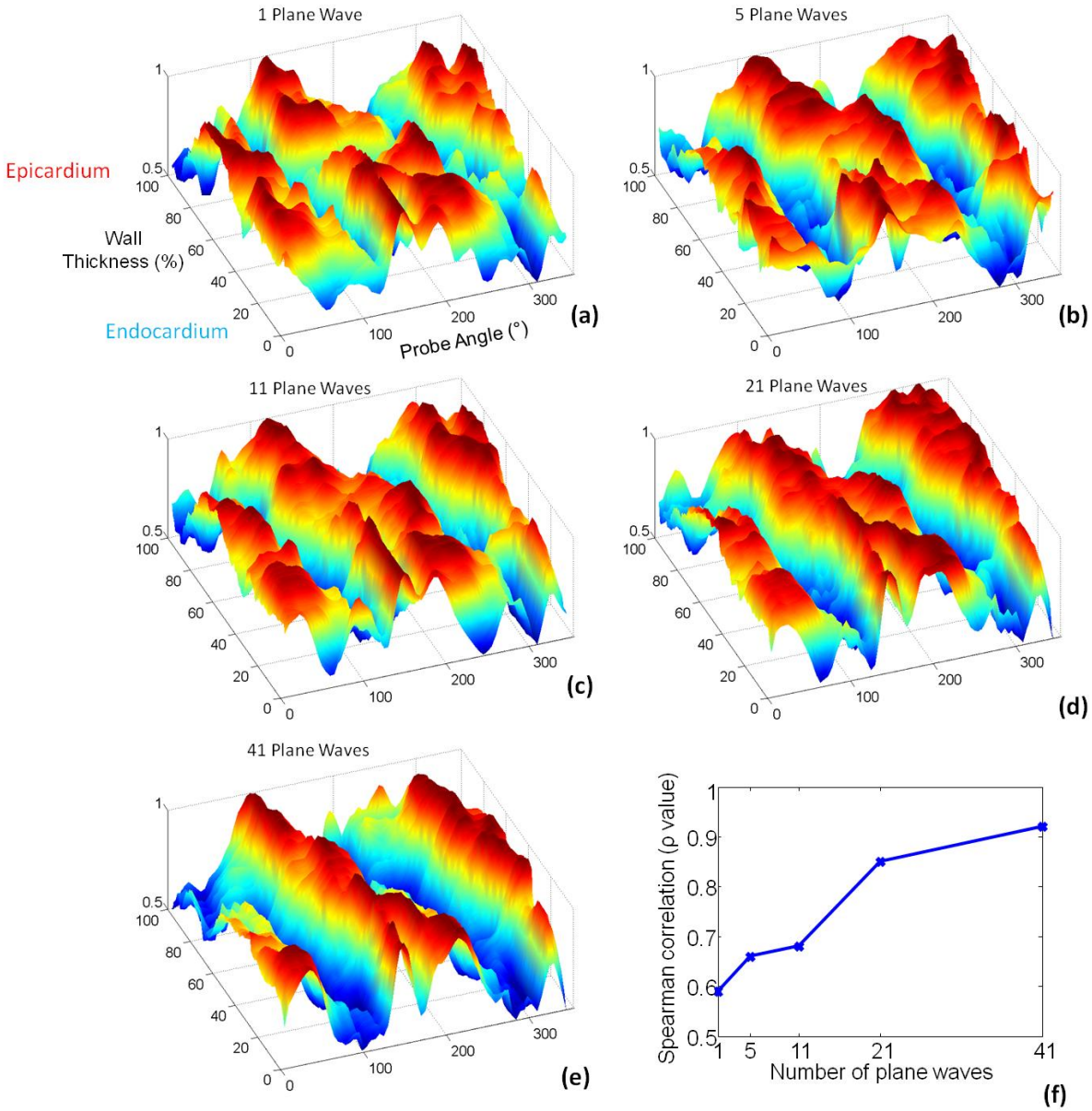

Fig.12. Normalized SACF as a function of probe angle for different number of plane waves 1,5,11,21,41 plane waves (a),(b),(c),(d),(e) respectively in a myocardial sample. Spearman correlation's coefficient of fiber angle estimated by ETI compared to BTI for a different number of plane waves used in coherent compound process is plotted (f).

A number as low as 5 transmits could be enough to obtain the estimation of the fiber directions ($\rho \approx 0.7$). This may enable us to increase the acquisition frame rate for real-time in vivo experiments and to reduce artifacts from coherent compound due to high tissue velocity.

IV. DISCUSSION

In this paper, spatial coherence of backscattered echoes wasanalyzed to investigate the anisotropy of soft tissues. As previously found by Derode et al. [38]in solid composite materials,we observeda strong anisotropy of spatial coherence in skeletal muscles as well as in myocardium. Based on this anisotropy, the direction of fibers of the skeletal muscle samples was successfully derived and significant FA were found. Moreover, the complex fiber distribution of myocardial samples was measured in good agreement with ETI, another technique previously developed to map the elastic anisotropy of myocardium. Although the two techniques rely on the anisotropy of different physical properties (i.e backscatter and elastic properties), this result is linked in both cases to the microstructure of the tissue, and provided comparable results in term of fiber orientation. ETI was already compared in *ex vivo* myocardial samples to magnetic resonance diffusion tensor imaging (MR-DTI), which measures the anisotropy of water diffusion, and similar fiber distribution was found by both techniques. Current clinical uses of MR DTI are strongly limited by long acquisition times, cost and complexity of MR scanners, so that ultrasound based techniques such as BTI and ETI may have strong clinical potential for real-time measurements in the myocardium. One advantage of BTI over ETI is the lower energy required to map an entire region because ETI relies on the generation of shear waves at multiple locations using the acoustic radiation force induced by long ultrasonic burstswhereas BTI relies only on pulse emissions.

Another original aspect of the method developed in this paper was the use of plane wave transmits to image the spatial coherence. Plane wave coherent compounding was used to synthetize a focus everywhere in the imaging plane in order to assess the coherence functions and the coherence factor at each point of space. In contrast to conventional transmit focusing, plane wave compounding presents several advantages for mapping the spatial coherence. First, a lower number of transmits is required to map the spatial coherence in 2D over the entire field of view. In this study, 41 plane waves were used but the number of plane waves could be reduced to increase the frame rate (e.g. Figure 12). When decreasing the number of transmits, the overall spatial coherence decreases because a larger focus are generated but the contrast of the coherence image remains high.

The results presented in this paper,are limited to the 1D mapping of the fiber distributionalong the rotation axis of the probe. Mapping the fiber distribution in 3D would require to mechanically scan the probe over the sample. However, using 2D matrix arrays the spatial coherence could be assessed in different directions using the same backscattered data, removing the need of rotation axis. Moreover, the plane wave approach could be extended in 3D which would provide the backscatter information over an entire volume. Thus, it may be possible with BTI to obtain in real-time 3D mapsof the microstructure of tissues. The fiber orientation detection is also limited to projected component of real fiber direction on the transducer surface plane. As long as the fibers are oriented parallel to the transducer surface plane, the real direction can be detected. However, to detect fibers with a certain angle regarding to the transducer surface plane, a Beamforming with subaperture strategy could be used[41].

In this study, a linear transducer with a central frequency of 6MHz was used. For cardiac applications with smaller aperture such as in transthoracic and transoesophagial echocardiography, plane wave coherent compounding could be replaced by diverging waves[42],[43]. The application to transoesophagial echocardiography is particularly interesting because most of the 2D transoesophagial transducers are mounted on a motorized rotation axis.

BTI could be implemented on any type of ultrasonic scanner with conventional probes and adapted sequences.Moreover, beyond cardiac applications, BTI could be used to map the anisotropy of fibrous tissues such as brain in transfontanellar imaging, skeletal muscle or tendon.

V. CONCLUSION

In this paper, spatial coherence of ultrasonic backscatter echoes from plane wave transmits was analyzed in anisotropic tissues. Plane wave coherent compounding enabled mapping the spatial coherence in 2D using a small number of emissions. We investigated the spatial coherence dependence with the probe orientation and showed the possibility to map the fibers distribution in soft tissues. This new technique called Backscatter Tensor Imaging (BTI),was used tomeasure the fibers orientation in (N=3) *ex vivo* bovine skeletal muscles and in (N=3) *ex vivo* porcine myocardial samples and compared it to the anisotropy measured by shear wave elastography. We demonstrated that BTI has the sensitivity to reveal the complex transmural fiber distribution in*ex vivo* myocardium. Finally, the spatial coherence dependence with the number of plane waves was investigated and a small number of transmitted plane waves was found sufficient to measure the tissue anisotropy and fiber direction. BTI has a strong potential to become a major tool to explore non-invasively the anisotropy *in vivo* in human hearts or in other anisotropic organs such including brain, tendon and skeletal muscles.

Acknowledgements

The research leading to these results has received funding from the European Research Council under the European Union's Seventh Framework Programme (FP/2007–2013) / ERC Grant Agreement n°311025

References

[1] D. D. Streeter and D. L. Bassett, “An engineering analysis of myocardial fiber orientation in pig’s left ventricle in systole,” *Anat. Rec.*, vol. 155, no. 4, pp. 503–511, 1966.

[2] T. Arts, K. D. Costa, J. W. Covell, and A. D. McCulloch, “Relating myocardial laminar architecture to shear strain and muscle fiber orientation,” *Am. J. Physiol.-Heart Circ. Physiol.*, vol. 280, no. 5, pp. H2222–H2229, 2001.

[3] K. D. Costa, Y. Takayama, A. D. McCulloch, and J. W. Covell, “Laminar fiber architecture and three-dimensional systolic mechanics in canine ventricular myocardium,” *Am. J. Physiol.-Heart Circ. Physiol.*, vol. 276, no. 2, pp. H595–H607, 1999.

[4] L. K. Waldman, D. Nosan, F. Villarreal, and J. W. Covell, “Relation between transmural deformation and local myofiber direction in canine left ventricle,” *Circ. Res.*, vol. 63, no. 3, pp. 550–562, Sep. 1988.

[5] D. A. Hooks, M. L. Trew, B. J. Caldwell, G. B. Sands, I. J. LeGrice, and B. H. Smaill, “Laminar Arrangement of Ventricular Myocytes Influences Electrical Behavior of the Heart,” *Circ. Res.*, vol. 101, no. 10, pp. e103–e112, Sep. 2007.

[6] A. Kadish, M. Shinnar, E. N. Moore, J. H. Levine, C. W. Balke, and J. F. Spear, “Interaction of fiber orientation and direction of impulse propagation with anatomic barriers in anisotropic canine myocardium,” *Circulation*, vol. 78, no. 6, pp. 1478–1494, Dec. 1988.

[7] D. E. Roberts, L. T. Hersh, and A. M. Scher, “Influence of cardiac fiber orientation on wavefront voltage, conduction velocity, and tissue resistivity in the dog,” *Circ. Res.*, vol. 44, no. 5, pp. 701–712, May 1979.

[8] B. Taccardi, E. Macchi, R. L. Lux, P. R. Ershler, S. Spaggiari, S. Baruffi, and Y. Vyhmeister, “Effect of myocardial fiber direction on epicardial potentials,” *Circulation*, vol. 90, no. 6, pp. 3076–3090, Dec. 1994.

[9] C. P. Fleming, C. M. Ripplinger, B. Webb, I. R. Efimov, and A. M. Rollins, “Quantification of cardiac fiber orientation using optical coherence tomography,” *J. Biomed. Opt.*, vol. 13, no. 3, p. 030505, 2008.

[10] H. Huang, C. Macgillivray, H.-S. Kwon, J. Lammerding, J. Robbins, R. T. Lee, and P. So, “Three-dimensional cardiac architecture determined by two-photon microtomy,” *J. Biomed. Opt.*, vol. 14, no. 4, p. 044029, Aug. 2009.

[11] E. W. Hsu, A. L. Muzikant, S. A. Matulevicius, R. C. Penland, and C. S. Henriquez, “Magnetic resonance myocardial fiber-orientation mapping with direct histological correlation,” *Am. J. Physiol.-Heart Circ. Physiol.*, vol. 274, no. 5, pp. H1627–H1634, 1998.

[12] D. F. Scollan, A. Holmes, R. Winslow, and J. Forder, “Histological validation of myocardial microstructure obtained from diffusion tensor magnetic resonance imaging,” *Am. J. Physiol.-Heart Circ. Physiol.*, vol. 275, no. 6, pp. H2308–H2318, 1998.

[13] T. G. Reese, R. M. Weisskoff, R. N. Smith, B. R. Rosen, R. E. Dinsmore, and V. J. Wedeen, “Imaging myocardial fiber architecture in vivo with magnetic resonance,” *Magn. Reson. Med. Off. J. Soc. Magn. Reson. Med. Soc. Magn. Reson. Med.*, vol. 34, no. 6, pp. 786–791, Dec. 1995.

[14] W.-Y. I. Tseng, J. Dou, T. G. Reese, and V. J. Wedeen, “Imaging myocardial fiber disarray and intramural strain hypokinesis in hypertrophic cardiomyopathy with MRI,” *J. Magn. Reson. Imaging*, vol. 23, no. 1, pp. 1–8, Jan. 2006.

[15] M.-T. Wu, W.-Y. I. Tseng, M.-Y. M. Su, C.-P. Liu, K.-R. Chiou, V. J. Wedeen, T. G. Reese, and C.-F. Yang, “Diffusion Tensor Magnetic Resonance Imaging Mapping the Fiber Architecture Remodeling in Human Myocardium After Infarction: Correlation With Viability and Wall Motion,” *Circulation*, vol. 114, no. 10, pp. 1036–1045, Aug. 2006.

[16] H. Rimington, *Echocardiography: A Practical Guide for Reporting*. CRC Press, 2007.

[17] J. G. Mottley and J. G. Miller, “Anisotropy of the ultrasonic attenuation in soft tissues: Measurements in vitro,” *J. Acoust. Soc. Am.*, vol. 88, no. 3, pp. 1203–1210, 1990.

[18] S. L. Baldwin, K. R. Marutyan, M. Yang, K. D. Wallace, M. R. Holland, and J. G. Miller, “Measurements of the anisotropy of ultrasonic attenuation in freshly excised myocardium,” *J. Acoust. Soc. Am.*, vol. 119, no. 5, p. 3130, 2006.

[19] S. A. Wickline, E. D. Verdonk, and J. G. Miller, “Three-dimensional characterization of human ventricular myofiber architecture by ultrasonic backscatter.,” *J. Clin. Invest.*, vol. 88, no. 2, p. 438, 1991.

[20] E. I. Madaras, J. Perez, B. E. Sobel, J. G. Mottley, and J. G. Miller, “Anisotropy of the ultrasonic backscatter of myocardial tissue: II. Measurements in vivo,” *J. Acoust. Soc. Am.*, vol. 83, no. 2, pp. 762–769, 1988.
[21] R. Sinkus, M. Tanter, S. Catheline, J. Lorenzen, C. Kuhl, E. Sondermann, and M. Fink, “Imaging anisotropic and viscous properties of breast tissue by magnetic resonance-elastography,” *Magn. Reson. Med.*, vol. 53, no. 2, pp. 372–387, 2005.
[22] J.-L. Gennisson, T. Deffieux, E. Macé, G. Montaldo, M. Fink, and M. Tanter, “Viscoelastic and Anisotropic Mechanical Properties of in vivo Muscle Tissue Assessed by Supersonic Shear Imaging,” *Ultrasound Med. Biol.*, vol. 36, no. 5, pp. 789–801, May 2010.
[23] J. Bercoff, M. Tanter, and M. Fink, “Supersonic shear imaging: a new technique for soft tissue elasticity mapping,” *IEEE Trans. Ultrason. Ferroelectr. Freq. Control*, vol. 51, no. 4, pp. 396–409, Apr. 2004.
[24] W.-N. Lee, M. Pernot, M. Couade, E. Messas, P. Bruneval, A. Bel, A. A. Hagège, M. Fink, and M. Tanter, “Mapping myocardial fiber orientation using echocardiography-based shear wave imaging,” *IEEE Trans. Med. Imaging*, vol. 31, no. 3, pp. 554–562, Mar. 2012.
[25] W.-N. Lee, M. Couade, C. Flanagan, M. Fink, M. Pernot, and M. Tanter, “Noninvasive assessment of myocardial anisotropy in vitro and in vivo using Supersonic Shear Wave Imaging,” in *2010 IEEE Ultrasonics Symposium (IUS)*, 2010, pp. 690–693.
[26] W.-N. Lee, B. Larrat, M. Pernot, and M. Tanter, “Ultrasound elastic tensor imaging: comparison with MR diffusion tensor imaging in the myocardium,” *Phys. Med. Biol.*, vol. 57, no. 16, pp. 5075–5095, Aug. 2012.
[27] M. Couade, M. Pernot, E. Messas, A. Bel, M. Ba, A. Hagege, M. Fink, and M. Tanter, “In vivo quantitative mapping of myocardial stiffening and transmural anisotropy during the cardiac cycle,” *IEEE Trans. Med. Imaging*, vol. 30, no. 2, pp. 295–305, Feb. 2011.
[28] M. Pernot, M. Couade, P. Mateo, B. Crozatier, R. Fischmeister, and M. Tanter, “Real-time assessment of myocardial contractility using shear wave imaging,” *J. Am. Coll. Cardiol.*, vol. 58, no. 1, pp. 65–72, Jun. 2011.
[29] C. Papadacci, M. Pernot, M. Couade, M. Fink, and M. Tanter, “Shear Wave Imaging of the heart using a cardiac phased array with coherent spatial compound,” in *Ultrasonics Symposium (IUS), 2012 IEEE International*, 2012, pp. 2023–2026.
[30] P. Song, H. Zhao, M. W. Urban, A. Manduca, S. V. Pislaru, R. R. Kinnick, J. F. Greenleaf, and S. Chen, “Robust shear wave motion tracking using ultrasound harmonic imaging,” *J. Acoust. Soc. Am.*, vol. 134, no. 5, p. 4010, Nov. 2013.
[31] R. Mallart and M. Fink, “The van Cittert–Zernike theorem in pulse echo measurements,” *J. Acoust. Soc. Am.*, vol. 90, no. 5, pp. 2718–2727, 1991.
[32] W. F. Walker and G. E. Trahey, “Speckle coherence and implications for adaptive imaging,” *J. Acoust. Soc. Am.*, vol. 101, no. 4, pp. 1847–1858, Apr. 1997.
[33] R. Mallart and M. Fink, “Adaptive focusing in scattering media through sound-speed inhomogeneities: The van Cittert Zernike approach and focusing criterion,” *J. Acoust. Soc. Am.*, vol. 96, no. 6, pp. 3721–3732, 1994.
[34] K. W. Hollman, K. W. Rigby, and M. O’donnell, “Coherence factor of speckle from a multi-row probe,” in *1999 IEEE Ultrasonics Symposium, 1999. Proceedings*, 1999, vol. 2, pp. 1257–1260 vol.2.
[35] P.-C. Li and M.-L. Li, “Adaptive imaging using the generalized coherence factor,” *IEEE Trans. Ultrason. Ferroelectr. Freq. Control*, vol. 50, no. 2, pp. 128–141, 2003.
[36] M. A. Lediju, G. E. Trahey, B. C. Byram, and J. J. Dahl, “Short-lag spatial coherence of backscattered echoes: imaging characteristics,” *IEEE Trans. Ultrason. Ferroelectr. Freq. Control*, vol. 58, no. 7, pp. 1377–1388, Jul. 2011.
[37] J. J. Dahl, M. Jakovljevic, G. F. Pinton, and G. E. Trahey, “Harmonic spatial coherence imaging: an ultrasonic imaging method based on backscatter coherence,” *IEEE Trans. Ultrason. Ferroelectr. Freq. Control*, vol. 59, no. 4, pp. 648–659, Apr. 2012.
[38] A. Derode and M. Fink, “Spatial coherence of ultrasonic speckle in composites,” *IEEE Trans. Ultrason. Ferroelectr. Freq. Control*, vol. 40, no. 6, pp. 666–675, 1993.
[39] M. Tanter and M. Fink, “Ultrafast imaging in biomedical ultrasound,” *IEEE Trans. Ultrason. Ferroelectr. Freq. Control, in press*, Jan. 2014.

[40] G. Montaldo, M. Tanter, J. Bercoff, N. Benech, and M. Fink, “Coherent plane-wave compounding for very high frame rate ultrasonography and transient elastography,” *IEEE Trans. Ultrason. Ferroelectr. Freq. Control*, vol. 56, no. 3, pp. 489–506, Mar. 2009.
[41] M. Tanter, J. Bercoff, L. Sandrin, and M. Fink, “Ultrafast compound imaging for 2-D motion vector estimation: application to transient elastography,” *IEEE Trans. Ultrason. Ferroelectr. Freq. Control*, vol. 49, no. 10, pp. 1363–1374, Oct. 2002.
[42] M. Karaman, P.-C. Li, and M. O’donnell, “Synthetic aperture imaging for small scale systems,” *IEEE Trans. Ultrason. Ferroelectr. Freq. Control*, vol. 42, no. 3, pp. 429–442, 1995.
[43] C. Papadacci, M. Pernot, M. Couade, M. Fink, and M. Tanter, “High-contrast ultrafast imaging of the heart,” *IEEE Trans. Ultrason. Ferroelectr. Freq. Control*, vol. 61, no. 2, pp. 288–301, Feb. 2014.